doi:10.1093/brain/awu138 Brain 2014: 137; 2329–2345 | 2329

BRAIN
A JOURNAL OF NEUROLOGY

A mitochondrial origin for frontotemporal dementia and amyotrophic lateral sclerosis through *CHCHD10* involvement

Sylvie Bannwarth,[1,2,*] Samira Ait-El-Mkadem,[1,2,*] Annabelle Chaussenot,[1,2] Emmanuelle C. Genin,[1] Sandra Lacas-Gervais,[3] Konstantina Fragaki,[1,2] Laetitia Berg-Alonso,[1] Yusuke Kageyama,[4] Valérie Serre,[5] David G. Moore,[6] Annie Verschueren,[7] Cécile Rouzier,[1,2] Isabelle Le Ber,[8,9] Gaëlle Augé,[1,2] Charlotte Cochaud,[2] Françoise Lespinasse,[1] Karine N'Guyen,[10] Anne de Septenville,[8] Alexis Brice,[8] Patrick Yu-Wai-Man,[6] Hiromi Sesaki,[4] Jean Pouget[7] and Véronique Paquis-Flucklinger[1,2]

1 IRCAN, UMR CNRS 7284/INSERM U1081/UNS, School of Medicine, Nice Sophia-Antipolis University, France
2 Department of Medical Genetics, National Centre for Mitochondrial Diseases, Nice Teaching Hospital, France
3 Joint Centre for Applied Electron Microscopy, Nice Sophia-Antipolis University, France
4 Department of Cell Biology, Johns Hopkins University School of Medicine, Baltimore, MD 21205, USA
5 UMR7592 CNRS, Jacques Monod Institute, Paris Diderot University, France
6 Wellcome Trust Centre for Mitochondrial Research, Institute of Genetic Medicine, International Centre for Life, Newcastle University, Newcastle upon Tyne NE1 3BZ, UK
7 Department of Neurology, Timone Hospital, Marseille Teaching Hospital, France
8 Sorbonne Université, UPMC Univ Paris 06, UM75, Inserm U1127, Cnrs UMR7225, Institut du Cerveau et de la Moelle épinière (ICM), F-75013 Paris, France
9 National Reference Centre on Rare Dementias, AP-HP, Groupe Hospitalier Pitié-Salpêtrière, Paris, France
10 Department of Medical Genetics, Timone Hospital, Marseille Teaching Hospital, France

*These authors contributed equally to this work.

Correspondence to: Prof. Véronique Paquis-Flucklinger,
IRCAN UMR CNRS 7284 / INSERM U1081 / UNS,
School of Medicine, 28 av de Valombrose,
06107 Nice cedex 2, France
E-mail: paquis@hermes.unice.fr

Mitochondrial DNA instability disorders are responsible for a large clinical spectrum, among which amyotrophic lateral sclerosis-like symptoms and frontotemporal dementia are extremely rare. We report a large family with a late-onset phenotype including motor neuron disease, cognitive decline resembling frontotemporal dementia, cerebellar ataxia and myopathy. In all patients, muscle biopsy showed ragged-red and cytochrome *c* oxidase-negative fibres with combined respiratory chain deficiency and abnormal assembly of complex V. The multiple mitochondrial DNA deletions found in skeletal muscle revealed a mitochondrial DNA instability disorder. Patient fibroblasts present with respiratory chain deficiency, mitochondrial ultrastructural alterations and fragmentation of the mitochondrial network. Interestingly, expression of matrix-targeted photoactivatable GFP showed that mitochondrial fusion was not inhibited in patient fibroblasts. Using whole-exome sequencing we identified a missense mutation (c.176C>T; p.Ser59Leu) in the *CHCHD10* gene that encodes a coiled-coil helix coiled-coil helix protein, whose function is unknown. We show that CHCHD10 is a mitochondrial protein located in the intermembrane space and enriched at cristae junctions. Overexpression of a *CHCHD10* mutant allele in HeLa cells led to fragmentation of the mitochondrial network and ultrastructural major abnormalities including loss, disorganization and dilatation of cristae. The observation of a frontotemporal

Received January 6, 2014. Revised March 18, 2014. Accepted April 6, 2014. Advance Access publication June 16, 2014

dementia-amyotrophic lateral sclerosis phenotype in a mitochondrial disease led us to analyse *CHCHD10* in a cohort of 21 families with pathologically proven frontotemporal dementia-amyotrophic lateral sclerosis. We identified the same missense p.Ser59Leu mutation in one of these families. This work opens a novel field to explore the pathogenesis of the frontotemporal dementia-amyotrophic lateral sclerosis clinical spectrum by showing that mitochondrial disease may be at the origin of some of these phenotypes.

Keywords: *CHCHD10*; mitochondrial DNA instability; mitochondrial disorder; FTD-ALS

Abbreviations: ALS = amyotrophic lateral sclerosis; COX = cytochrome *c* oxidase; FTD = frontotemporal dementia; mitoPAGFP = mitochondria-targeted photoactivatable GFP

Introduction

Mitochondrial disorders can result from defects in mitochondrial DNA or in nuclear genes that encode proteins that are imported in the mitochondria. In recent years, a growing list of genes responsible for mitochondrial DNA instability has been reported (Copeland, 2012; Shapira, 2012; Ylikallio and Suomalainen, 2012). Mutations in these genes lead either to mitochondrial DNA depletion syndrome, a devastating mitochondrial disease of childhood associated with a significant reduction of mitochondrial DNA copy number, or disorders characterized by accumulation of multiple mitochondrial DNA deletions in post-mitotic tissues (Suomalainen and Isohanni, 2010; Copeland, 2012). Diseases associated with deletions comprise commonly known clinical presentations including progressive external ophthalmoplegia and ataxia neuropathy syndromes, but also some rare disorders (for review see Copeland, 2012). To date, nuclear genes responsible for mitochondrial DNA instability disorders mainly fall into three categories: (i) genes encoding proteins directly involved in mitochondrial DNA replication, such as *POLG*, *POLG2* or *C10orf2* (formerly known as twinkle); (ii) genes encoding proteins responsible for the maintenance of mitochondrial nucleotide pool, such as *TMPO* (formerly known as *TP*), *TK2*, *DGUOK*; and (iii) genes encoding membrane proteins involved in mitochondrial dynamics, such as *OPA1* or *MFN2* (Amati-Bonneau *et al*., 2008; Hudson *et al*., 2008; Rouzier *et al*., 2012). This third category was recently individualized. Autosomal dominant optic atrophy is mainly related to mutations in the *OPA1* gene, which encodes a dynamin-like GTPase involved in the fusion of the inner mitochondrial membrane (Delettre *et al*., 2000). MFN2 is one of the two mitofusin proteins also required for mitochondrial fusion. MFN1 and MFN2 are conserved integral outer mitochondrial membrane proteins, each consisting of a large GTPase domain and 2 heptad repeat (HR), or putative coil-coiled domains, all of which face the cytoplasm (Koshiba *et al*., 2004; Meeusen *et al*., 2004; Song *et al*., 2009). *MFN2* mutations are a major cause of primary axonal Charcot–Marie–Tooth disease type 2A (CMT2A) (Zuchner *et al*., 2004), an autosomal dominant neuropathy that impairs motor and sensory neurons with the longest axons resulting in earliest symptoms in distal extremities. A subset of *OPA1* missense mutations have been associated with the 'autosomal dominant optic atrophy plus' syndrome and with accumulation of mitochondrial DNA deletions in muscle (Amati-Bonneau *et al*., 2008; Hudson *et al*., 2008). Complex phenotypes have also been associated with *MFN2* mutations. Recently, we reported a large family with optic atrophy beginning in early childhood, associated with axonal neuropathy and mitochondrial myopathy with mitochondrial DNA deletions in adult life. The clinical presentation resembles the autosomal dominant optic atrophy plus phenotype linked to *OPA1* mutations, but is associated with a novel *MFN2* missense mutation, thus confirming the link between mitochondrial DNA stability and mitochondrial fusion (Rouzier *et al*., 2012).

Here, we report the involvement of a novel gene responsible for 'mitochondrial DNA breakage' syndrome and frontotemporal lobe dementia-amyotrophic lateral sclerosis (FTD-ALS) through two families of French and Spanish origin. The responsible gene, *CHCHD10*, encodes a coiled-coil helix coiled-coil helix protein whose function is unknown. However, CHCHD10 belongs to a family of mitochondrial proteins located in the intermembrane space, some of which interact with OPA1 and are involved in cristae integrity and mitochondrial fusion (Darshi *et al*., 2011; An *et al*., 2012).

Materials and methods

Patients

The pedigree of the first family of French origin is shown in Fig. 1. All clinical data are summarized in Table 1. Blood and tissue samples were obtained after patients had given informed consent. The index case was a 67-year-old female (Patient IV-6), who developed a cerebellar ataxia at 50 years of age, associated with progressive bulbar syndrome, dementia and sensorineural deafness. Clinical examination showed cerebellar ataxia, Babinski sign, areflexia and bulbar palsy with dysarthria and dysphagia. Neuropsychological tests revealed a frontal lobe syndrome. Laboratory investigations showed normal lactate concentrations (1.6 mmol/l, normal <2.1 mmol/l). She died at 67 years of age.

The age of onset of the seven other patients who underwent a muscle biopsy was between 49 and 65 years. Three patients presented with a motor neuron disease, two with cerebellar ataxia and the two last patients had a motor neuron disease and a cerebellar ataxia, similar to the index case. All developed cognitive disorders with mainly a frontal lobe syndrome, except Patient V-2 who died at age 51. Neuropsychological evaluation of Patient IV-3 showed severe impairment in episodic memory, attention, verbal fluency and executive functions with behavioural changes corresponding to frontal dementia. Brain MRI of Patient V-10 was normal, and Patient IV-3 showed moderate cortical atrophy. Brain MRI performed in four other patients

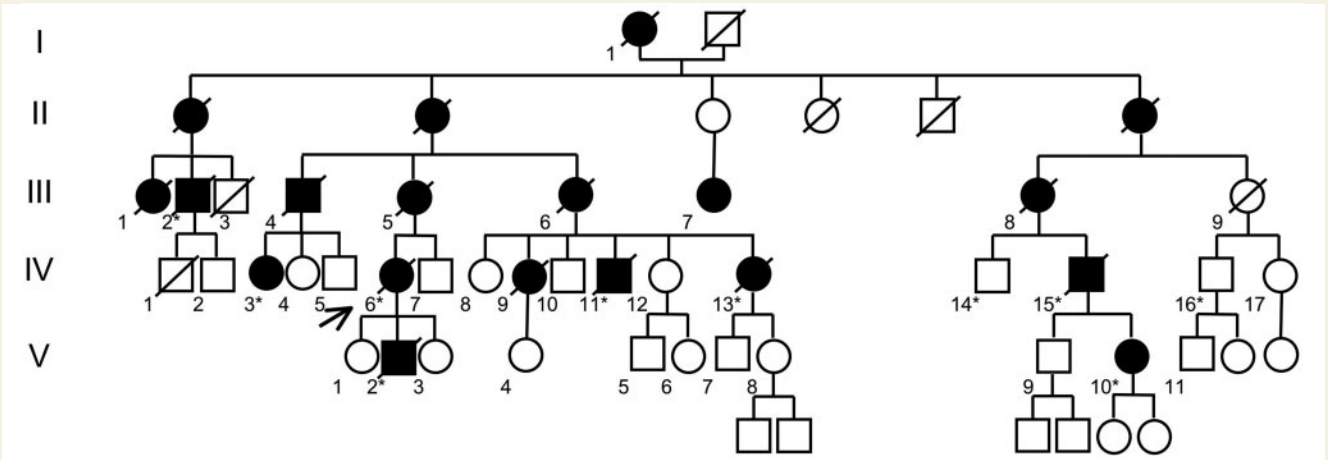

Figure 1 Pedigree of the first family. Solid symbols represent clinically affected individuals. Asterisk corresponds to individuals tested for segregation analysis.

(Patients III-2, IV-11, IV-13 and V-2) showed no specific abnormality. Proximal weakness was observed in four individuals (Patients IV-3, IV-11, IV-13 and IV-15) with bilateral ptosis and facial paresis in Patient IV-15. Electromyography excluded peripheral neuropathy with normal test (Patient V-10), chronic neurogenic changes suggesting a lower motor neuron disease (Patient IV-15) or myopathic abnormalities only (Patient IV-3). Patients IV-3 and V-10 are alive at the time of writing, all others died after >10 years of evolution.

Other affected individuals had no muscle biopsy (Patients I-1, II-1, II-2, II-6, III-1, III-4, III-5, III-6, III-7, III-8 and IV-9). They presented dementia, progressive bulbar syndrome with dysarthria and dysphagia, and became bedridden.

Muscle histopathology and ultrastructure

Muscle samples were frozen in cooled isopentane and stored in liquid nitrogen for histological and histoenzymatic analysis including Gomori modified trichrome staining, cytochrome *c* oxidase (COX) activity, succinate dehydrogenase (SDH) activity and double COX/SDH staining according to standard protocols. A fragment of muscle was also fixed in 2% glutaraldehyde and processed for ultrastructural analysis by electron microscopy.

Oxidative phosphorylation spectrophotometric measurements

Enzymatic spectrophotometric measurements of the oxidative phosphorylation respiratory chain complexes and citrate synthase were performed at 37°C on crude muscle homogenates and fibroblasts according to standard procedures (Rustin *et al*., 1994).

Polarographic study

Polarographic studies on fibroblasts of intact cell respiration and digitonin (0.004%) permeabilized cells mitochondrial substrate oxidation were carried out as previously described (Rustin *et al*., 1994).

Blue native gel electrophoresis and immunoblotting

Fifteen micrograms of muscle mitochondrial respiratory complexes, obtained by solubilization in a solution of 1.5 M aminocaproic acid (Sigma-Aldrich), 75 mM Bis-TRIS (Sigma-Aldrich) and 4% dodecyl-β-D-maltoside (Sigma-Aldrich), were separated by blue native-PAGE on a 4–13% acrylamide gradient gel (Schägger and Pfeiffer, 2001). Samples were then electroblotted onto a PVDF membrane before sequential incubation with specific antibodies directed against GRIM19 subunit of complex I, SDHA subunit of complex II, UQCRC2 subunit of complex III, MTCO1 subunit of complex IV and ATP5A subunit of complex V (Mitosciences) allowing us to verify that samples were equally loaded between patients and controls.

Protein measurement

Proteins were measured according to Bradford microassay (Bradford, 1976).

Mitochondrial DNA molecular analysis

Total DNA was extracted using standard phenol chloroform procedure. Long-range PCR and Southern blot analysis were performed as previously described (Moraes *et al*., 1989; Paul *et al*., 1996). Mitochondrial DNA quantification in muscle was performed by real-time quantitative PCR as described by Rouzier *et al*. (2010). Primer sequences and PCR conditions are available on request.

Sequencing of nuclear genes

The coding regions of *POLG* (NM_002693.2), *SLC25A4* (ANT1) (NM_001151.3) and *C10orf2* (Twinkle) (NM_021830.4) genes were sequenced as previously described (Naimi *et al*., 2006). PCR products were purified with illustra™ ExoStar™ enzyme (GE Healthcare), processed with an ABI PRISM® dRhodamine Terminator Cycle Sequencing Ready Reaction kit (Applied Biosystems) and analysed on an ABI 3130XL automated sequencer (Applied Biosystems).

Table 1 Clinical data of affected members

Patient	III-2	IV-3	IV-6	IV-11	IV-13	IV-15	V-2	V-10
Sex	M	F	F	M	F	M	M	F
AO (years)	?	65	50	58	60	50	50	49
AB (years)	78	68	67	63	62	75	50	50
AD (years)	† ?	-	67	70	† ?	77	51	-
Syndromic diagnosis	MND	MND + cerebellar syndrome	MND + cerebellar syndrome	MND	Cerebellar syndrome	MND + cerebellar syndrome	MND with ALS-like	Cerebellar syndrome
Cerebellar ataxia	-	+	+	-	+	+	-	+
Dysarthria	Bulbar	Bulbar	Bulbar + cerebellar	Bulbar	Cerebellar	Bulbar	Bulbar	Cerebellar
Dysphagia	Bulbar	Bulbar	Bulbar	Bulbar	-	Bulbar	Bulbar	-
Areflexia	+	+	+	?	?	+	+	+
Babinski sign	+	+	+	-	+	+	-	+
Cognitive impairment	+	+	+	+	+	+	-	+
Others	Deafness	Proximal weakness	Deafness	Proximal weakness	Proximal weakness, neurogenic bladder	Proximal weakness, ptosis, facial paresis	-	-
Muscle histology	RRF + + COX−	RRF + + COX−	RRF 30% COX− Lipid and glycogen accumulation	RRF 30% COX− 40% Lipid and glycogen accumulation	RRF 30% COX− Lipid accumulation	RRF + + COX− Lipid accumulation	RRF 20% COX− 20% Lipid accumulation	RRF + + COX− 15% Lipid and glycogen accumulation
Respiratory chain analysis	↓CI, ↓CIV(m)	↓CIII (m)	↓CI, ↓CIV (m)	↓CI, ↓CIV (m)	Not done	Normal (m)	↓CI, ↓CIII, ↓CIV, ↓CV (m)	Normal (m)
Mitochondrial DNA deletions	+ (m)	+ (m)	+ (m)	+ (m)	+ (m)	+ (m)	+ (m)	+ (m)

M = male; F = female; AO = age at onset; AB = age at biopsy; AD = age of death; † = deceased; ? = unknown; m = muscle; MND = motor neuron disease; RRF = ragged-red fibres; COX− = COX-negative fibres; ↓ = decreased; + = present; - = absent.

Cell culture

Skin punches were obtained from Patient V-10 after informed consent. Primary fibroblast cultures were established using standard procedures in RPMI supplemented with 10% foetal bovine serum, 45 μg/ml uridine and 275 μg/ml sodium pyruvate. Cultures were incubated at 37°C with 5% CO_2. For galactose conditions, medium was replaced 24 h before experiments by glucose-free medium containing 5 mM galactose and 5 mM pyruvate (Zanna *et al*., 2008).

HeLa cells were maintained in Dulbecco's modified Eagle medium supplemented with penicillin (100 U/ml)/streptomycin (0.1 mg/ml), 10% foetal calf serum, at 37°C in a humidified atmosphere with 5% CO_2 in air. For transient transfections, HeLa cells were transfected using Lipofectamine™ 2000 (Invitrogen) according to the manufacturer's instructions.

Mitochondrial network analysis

For mitochondrial staining, cells were incubated in a 100 nM solution of MitoTracker® red (Invitrogen) for 15 min, medium was replaced by HeLa cells culture medium incubated 2 h at 37°C and washed in PBS. The samples were fixed with 4% paraformaldehyde (Electron Microscopy Sciences), washed with PBS, and mounted on glass slides using ProLong® Gold Antifade Reagent (Molecular Probes). For immunostaining, cells were fixed with 4% paraformaldehyde, washed five times with PBS and permeabilized with 2% Triton™ X-100. After PBS washing, coverslips were incubated with 5% bovine serum albumin for 30 min at room temperature before adding mouse anti-FlagM2 (Agilent Technologies) (1/2000 antibody diluted with PBS + bovine serum albumin 5%), mouse anti-HA (Cell Signaling) (1/100 antibody diluted with PBS-bovine serum albumin 5%) or rabbit anti-FlagM2 (Cell Signaling) (1/800 antibody diluted with PBS-bovine serum albumin 5%). The samples were incubated at room temperature for 1 h, PBS washed, and then incubated with fluorescent secondary antibody goat anti-mouse Alexa Fluor® 488 (Life Technologies) (1/1000 antibody diluted with PBS-bovine serum albumin 1%) or antibody goat anti-rabbit Alexa Fluor® 647 (Life Technologies) (1/1000 antibody diluted with PBS-bovine serum albumin 1%) for 1 h at room temperature. The coverslips were washed five times with PBS, mounted on glass slides using ProLong® Gold Antifade Reagent (Molecular Probes) and analysed using a Zeiss LSM510 meta confocal laser-scanning microscope.

The images were deconvolved with Huygens Essential Software™ (Scientific Volume Imaging) using a theoretically calculated point spread function for each of the dyes. All selected images were iteratively deconvolved with a maximum iteration scored 40 and a quality threshold at 0.05. The deconvolved images were used for quantitative mitochondrial network analysis with Huygens Essential Software™ with the following standardized set of parameters: threshold = 25% and seed = 0% for each cell types and garbage = 5 or 10 for HeLa cells and fibroblasts, respectively. The quantitative data were further analysed in Microsoft Excel and GraphPad Prism 5 (GraphPad Software). Mitochondrial network length was quantified for 35 randomly-selected individual cells.

Data are represented as mean ± SEM. Statistical analyses were performed by Student's unpaired *t*-test using GraphPad Prism 5 (GraphPad Software).

Exome sequencing

Genomic DNA was extracted from blood and 3 μg were fragmented by sonication. Exome targets were enriched with the SureSelect Human All Exon v4 + UTR – 70 Mb Kit (Agilent technologies) and sequenced on the Illumina HiSEQ 2000 platform (Illumina). Raw image files were processed by the Illumina Real Time Analysis pipeline for base calling and generating the read sets. The bioinfomatic analysis of sequencing data was based on the Illumina CASAVA pipeline (v1.8). CASAVA performs alignment of the 2 × 75 bp paired-end sequence reads to the hg19 reference genome, calls the SNPs based on the allele calls and read depth, and detects variants (single nucleotide polymorphisms and insertions/deletions). The alignment algorithm used was ELANDv2e. Only the positions included in the bait coordinates were conserved. The web application ERIS (Integragen) was used for data visualization and prioritization of variants.

For mutation validation and segregation analysis, a part of *CHCHD10* (NM_213720.1) spanning the mutation site in exon 2 was amplified with the following primers: 5′-TCGGGCCAGCC GGGGCTC-3′ (forward); and 5′-GGAAGCCTGCCTCTAAGTGA-3′ (reverse). Purification and sequencing of PCR products were performed as described above.

Homology modelling of human CHCHD10

Using the threading program PHYRE2 (Kelley and Sternberg, 2009), 142 residues of CHCHD10 (Met1 to Pro142) were modelled using CHCHD5 as template (PDB ID: 2LQL). Swiss-Pdb Viewer 3.7 (http://www.expasy.org/spdbv) was used to analyse the structural insight into CHCHD10 mutation and visualize the structure.

Plasmid constructions

The human full-length *CHCHD10* complementary DNA was amplified by reverse transcriptase PCR from total RNA of patient fibroblasts by using Transcription First strand cDNA synthesis kit (Roche) and Taq PCRx® DNA polymerase (Invitrogen).

We used the following primers: 5′-GGATCCACCGCCGCCACCATG-3′ (forward); and 5′-CTCGAGGGGCAGGGAGCTCAG-3′ (reverse) containing BamHI and XhoI restriction sites, respectively. Restriction-digested PCR products were cloned into pCMV-3tag-3A to generate Flag-tagged CHCHD10. Sequencing of the clones obtained led to the identification of plasmids coding for wild-type ($CHCHD10^{WT}$) and mutant ($CHCHD10^{S59L}$) complementary DNAs.

Western blotting

Total protein extracts (5–25 μg) were separated on acrylamide-SDS gels and transferred to PVDF membranes (Millipore). Specific proteins were detected by using mouse anti-MFN2 (1/2000, Abcam, #ab56889), anti-VDAC1 (1/2000, Millipore, #MABN504), anti-Flag M2 (1/2000, Agilent Technologies, #200412), anti-PCNA (1/5000, BD Biosciences, #610664), rabbit polyclonal anti-mitofilin (1/2000; Proteintech #10179-1-AP), anti-GAPDH (1/20 000, Abcam #ab9485), anti-β tubulin (1/10 000, Sigma-Aldrich, #T4026), anti-SMAC (1/4000, Abcam #ab8114), anti-TOM 20 (1/5000, BD Biosciences, #612278), anti-CHCHD10 (1/500, Sigma-Aldrich #HPA003440) and goat polyclonal anti-HSP60 (1/4000, Santa Cruz, #sc-1052) antibodies. Anti-mouse, anti-rabbit or anti-goat secondary antibody (Dako) was used at 1/10 000 and signals were detected using a chemiluminescence system (Immobilon Western HRP Chemilumiscent substrates, Millipore). Human multiple tissue blot was used as described by the manufacturer (G-Biosciences).

Isolation of mitochondria and mitoplast preparation

Mitochondria were isolated from HeLa transfected cells using Q-Proteome mitochondria isolation kit (Qiagen) as described by the manufacturer. Mitochondria were treated with proteinase K (Invitrogen) in the presence or absence of 0.2% Triton™ X-100 as described in Bannwarth *et al*. (2012). To prepare the mitoplasts, we used a digitonin treatment. Briefly, purified mitochondria were suspended in suspension buffer (250 mM sucrose, 1 mM EDTA, 20 mM HEPES-NaOH, pH 7.4). Mitochondria were treated with digitonin (2 mg/ml) for 15 min at room temperature. The resulting mitoplasts were treated for 10 min at room temperature with proteinase K (100 ng/μl). Proteolysis was halted by the addition of 10 mM PMSF (Sigma-Aldrich) for 15 min on ice. Laemmli sample buffer was added directly to samples, boiled and loaded on SDS-PAGE gels.

Alkali extraction of intact mitochondria

Alkali extraction was performed as previously described (Bannwarth *et al*., 2012). Briefly, intact isolated mitochondria (25 μg) were treated with 0.1 M Na_2CO_3 (pH 11.5) for 30 min on ice, and then centrifuged at 16 000*g* for 15 min at 4°C. Supernatants were retained and pellets were washed once and then resuspended in an equivalent volume of homogenization buffer (250 mM sucrose, 1 mM EDTA, 20 mM HEPES-NaOH pH 7.4, plus protease inhibitor). Equivalent volumes were analysed by immunoblot.

Immunoelectron microscopy

Cells were fixed with 2% paraformaldehyde, 0.2% glutaraldehyde in 0.1 M phosphate buffer (pH 7.4) for 2 h and were processed for ultracryomicrotomy according to a slightly modified Tokuyasu method (Tokuyasu, 1973). In brief, cell suspension was spun down in 10% gelatin. After immersion in 2.3 M sucrose [in (pH 7.4), 0.1 M phosphate buffer] overnight at 4°C, the samples were rapidly frozen in liquid nitrogen. Ultrathin (70-nm thick) cryosections were prepared with an ultracryomicrotome (Leica EMFCS) and mounted on formvar-coated nickel grids (Electron Microscopy Sciences). Immunostainings were processed with an automated immunogold labelling system Leica EM IGL as follows: the grids were incubated successively in PBS containing 50 mM NH4Cl (5 min twice), PBS containing 1% bovine serum albumin (5 min twice), PBS containing rabbit anti-CHCHD10 (Sigma-Aldrich) or anti-Hsp60 (Abcam, #ab46798) antibody in 1% bovine serum albumin for 1 h, PBS containing 0.1% bovine serum albumin (5 min, three times), PBS containing 1% bovine serum albumin and 10 nm colloidal gold conjugated protein AG (CMC), PBS containing 0.1% bovine serum albumin for 5 min, PBS for 5 min twice. Lastly, the samples were fixed for 10 min with 1% glutaraldehyde, rinsed in distilled water and were contrasted with a mixture of 1.8% methylcellulose and 0.3% uranyl acetate on ice. After having been dried in air, sections were examined under a JEOL 1400 transmission electron microscope.

Mitochondrial fusion assay

Mitochondrial fusion was examined using mitochondria-targeted photoactivatable GFP (mitoPAGFP), as described (Karbowski *et al*., 2004). The matrix-targeted presequence from Su9 (Wakabayashi *et al*., 2009) was fused to the N-terminus of photoactivatable GFP (Addgene #11910) and cloned into the lentiviral vector pHR-SIN (Kim *et al*., 2011). Fibroblasts were infected with lentiviral particles carrying mitoPAGFPz. Thirty minutes before observation, fibroblasts were stained with 7 nM tetramethylrhodamine ethyl ester to visualize mitochondria. mitoPAGFP was photoactivated by 405-nm light (30% power, three times) in a small region (30 × 30 pixels) using a Zeiss 780 LSM confocal microscope with an environmentally controlled chamber. Images were taken at 15-min intervals for 60 min. Fluorescence intensity of mitoPAGFP was quantified using NIH ImageJ.

Results

Mitochondrial myopathy with multiple mitochondrial DNA deletions

Muscle biopsy was performed in eight patients after informed consent (Patients III-2, IV-3, IV-6, IV-11, IV-13, IV-15, V-2 and V-10) (Fig. 1). Muscle analysis of the index case (Patient IV-6) showed typical features of mitochondrial myopathy including intracellular lipid accumulation with COX-negative and ragged-red fibres (30%) (Fig. 2A and B). Electron microscopy showed altered morphology of mitochondria and cristae organization with paracristalline inclusions (Fig. 2C). Similar findings with numerous ragged-red fibres and COX-deficient fibres were found in all patients tested. Spectrophotometric analysis showed a combined respiratory chain deficiency in most patients (Table 1). Blue native PAGE assay of Patients IV-3 and V-2 revealed smaller bands with antibody against complex V corresponding to assembly defect or increased instability (Fig. 2D). All patients carried multiple mitochondrial DNA deletions in muscle identified by both long range PCR (not shown) and Southern blot analysis (Fig. 2E). The determination of relative mitochondrial DNA copy number was performed by real-time quantitative PCR without finding any depletion (not shown).

Respiratory chain deficiency, abnormal mitochondrial network and mitochondrial ultrastructural alterations in patient fibroblasts

Spectrophotometric analysis of fibroblasts from Patient V-10 cultivated in glucose medium revealed no respiratory chain deficiency and polarographic analysis showed normal oxygen consumption and mitochondrial substrate oxidation (Table 2). In a glucose-free medium containing galactose, cells are forced to rely predominantly on oxidative phosphorylation for ATP production because the carbon source feeds the glycolytic pathway with a low efficiency. In galactose medium, spectrophotometric analysis revealed a multiple respiratory chain deficiency in patient fibroblasts and polarographic analysis showed a decrease of oxygen consumption, glutamate/malate and succinate (Table 2). Blue native-PAGE analysis of patient fibroblasts revealed no abnormality including complex V (not shown), the activity of which was normal by spectrophotometry. Multiple mitochondrial DNA deletions were not observed and the determination of relative mitochondrial

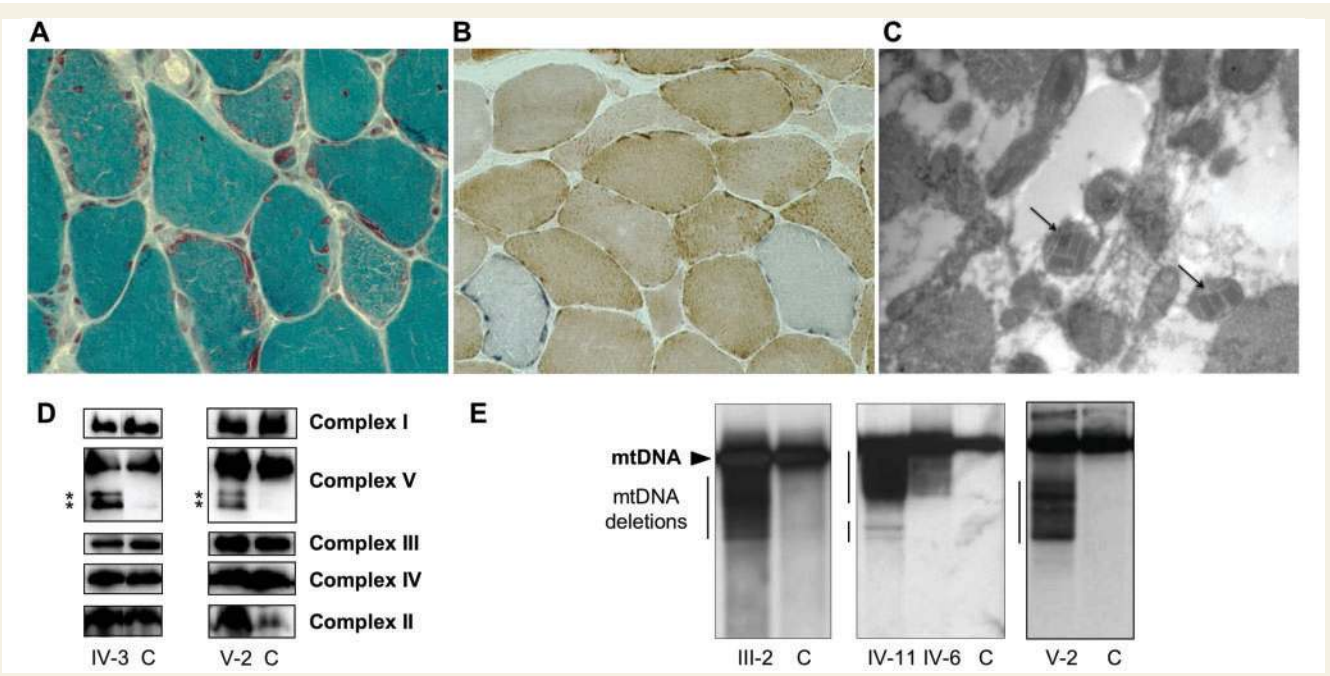

Figure 2 Muscle analysis. (**A** and **B**) Histopathology with Gomori modified trichrome (**A**) showing ragged-red fibres and COX/SDH stain (**B**) revealing COX-deficient fibres, which are recognized by the prevalent blue stain. (**C**) Ultrastructure of skeletal muscle showing abnormal mitochondria with crystalloid inclusions (arrows). (**D**) Blue native electrophoresis of muscle homogenates. Equal amounts (15 μg) of mitochondrial protein from age-matched control subjects (**C**) and Patients IV-3 and V-2 were subjected to blue native-PAGE, blotted onto a PVDF membrane and then incubated with specific antibodies. Asterisk corresponds to supplementary bands detected by anti-complex V antibody. (**E**) Southern blot analysis revealing multiple deletion bands in addition to wild-type fragments in muscle of Patients III-2, IV-11, IV-6 and V-2. C = control individual.

DNA copy number was performed by real-time quantitative PCR without finding any depletion (not shown).

We also compared the mitochondrial morphology of fibroblasts from Patient V-10 with that obtained from control fibroblasts. After staining with MitoTracker® and examination by confocal microscopy, control fibroblasts in glucose medium displayed a typical filamentous interconnected network. Patient fibroblasts presented with a fragmentation of the mitochondrial network and less connected mitochondria (Fig. 3A and B). We obtained the same results in galactose medium (not shown).

We then performed ultrastructural analysis of patient fibroblasts. Typical mitochondria of control cells had numerous, thin, well-defined cristae, running perpendicularly to the mitochondrial longitudinal axis, and with a regular pattern of parallel organization (Fig. 3C). They represented 90% of the mitochondrial profiles seen in two independent, genotype-blind, analyses of control cells. In patient cells, they represented 35% of the mitochondrial profiles. Completely disorganized mitochondria with sparse or absent cristae without recognizable parallel orientation were only observed in patient fibroblasts (18%) (Fig. 3D). Less disorganized mitochondria represented 47% of the mitochondrial pattern in patient cells and 10% in control cells (Fig. 3E).

No mitochondrial fusion defect in patient fibroblasts

The fragmentation of mitochondrial network observed in patient fibroblasts can be of different origins including a fusion deficiency. Furthermore, genes like *MFN2* or *OPA1* involved in mitochondrial fusion are responsible for complex neurological phenotypes associated with mitochondrial DNA deletions. To examine mitochondrial fusion, we expressed matrix-targeted photoactivatable GFP in control and patient fibroblasts (Karbowski *et al*., 2004). After photoactivation of mitoPAGFP in a portion of mitochondria, we monitored mixing of the fluorescent matrix marker. We found that the fluorescence intensity of mitoPAGFP similarly decreased for 60 min in both fibroblasts, suggesting that mitochondrial fusion is not inhibited in patient fibroblasts (Fig. 4).

Identification of a missense mutation in the *CHCHD10* gene by exome sequencing

Analysis of genes involved in multiple mitochondrial DNA deletions with a compatible phenotype (*POLG*, *SLC25A4*, *C10orf2*) revealed no mutation. To identify the causative gene, we sequenced the exome of Patients IV-11 and V-10. The procedure yielded 9.8 and 12.4 Gb of mappable sequence and after alignment to the hg19 reference genome, the average depth was ~70× and ~91×, respectively. From the 62 252 and 63 036 identified single nucleotide polymorphisms in Patients IV-11 and V-10, respectively, the pathogenic variant was identified by the following scheme: (i) selection of heterozygous variants shared by the two patients; (ii) exclusion of polymorphic variants present in dbSNP132, EVS

Table 2 Respiratory chain analysis in patient fibroblasts

Spectrophotometric analysis on fibroblasts						
Enzymatic activities	**I**	**II**	**III**	**IV**	**V**	**CS**
Glucose medium						
Control values (nmol/min/mg of proteins)	9.0–27.1	18.5–54.0	57.4–176.2	109.9–350.0	22.0–46.2	74.7–161.1
Patient V-10	16.8	29.7	112.3	202.7	29.7	125.6
Galactose medium						
Control values (nmol/min/mg of proteins)	15.2–19.4	28.2–33.1	88.8–116.4	181.7–315.4	22.7–32.1	124.8–223.0
Patient V-10	**10.0**	**26.7**	**60.2**	**167.1**	28.2	177.0
Oxygraphic analysis on fibroblasts						
Glucose medium						
	Oxygen consumption					
	Intact cells	**Digitonin permeabilized cells**				
		Glutamate + malate	**Succinate**	**G3P**		
Control values (nmol O_2/min/mg of proteins)	5.90–13.80	8.00–16.60	8.00–15.80	4.90–13.50		
Patient V-10	9.40	15.36	9.40	7.04		
Galactose medium						
	Oxygen consumption					
	Intact cells	**Digitonin permeabilized cells**				
		Glutamate + malate	**Succinate**	**G3P**		
Control values (nmol O_2/min/mg of proteins)	5.58–8.25	8.16–9.91	8.60–9.76	5.22–12.91		
Patient V-10	**4.66**	**6.22**	**7.82**	8.31		

Spectrophotometric and polarographic analysis of the respiratory chain enzyme activities in patient fibroblasts in glucose and in galactose medium. CS = citrate synthase; G3P = glycerol 3-phosphate. Results are expressed as extreme absolute values or absolute values for controls or patients, respectively. Values are expressed in nanomols of substrate per minute per milligram of proteins (lowered values are in bold).

(Exome Variant Server), HapMap, 1000 Genome databases and in-house control exomes; and (iii) segregation analysis within the family. This filtering led us to identify a single heterozygous missense mutation (c.176C>T; p.Ser59Leu) in exon 2 of *CHCHD10* that was present in the eight patients tested and was absent in two healthy individuals (Subjects IV-14 and IV-16) with normal neurological examination at 79 and 69 years, respectively (Fig. 5A and B). This gene encodes the coiled-coil helix coiled-coil helix domain-containing protein 10 whose function is unknown. However, the C-terminal CHCH domain is primarily seen in mitochondrial proteins and was known to be involved in the protein import and metal binding in the intermembrane space (Banci *et al*., 2009). The mutation changes a highly conserved serine into a leucine and was not present in 200 ethnically and geographically matched control alleles (Fig. 5C). *In silico* study by PolyPhen-2 (http://genetics.bwh.harvard.edu/pph2/), SIFT (http://sift.jcvi.org/) and Mutation Taster (http://www.mutationtaster.org/) predicted this variant to be probably damaging.

The CHCH domain of CHCHD10 is characterized by a CX_9C motif. Although all CX_9C proteins presumably preserve a disulphide bonded α-hairpin conformation, they have a large range of sequence lengths and a very low degree of sequence similarity both within or specific organism and the orthologues of different species (Longen *et al*., 2009; Cavallo, 2010). Therefore, these features do not allow us to easily predict accurate structural models for this protein family. Recently, Banci *et al*. (2012) have structurally characterized two members, CHCHD5 and CHCHD7, in their fully oxidized states (Banci *et al*., 2012). Using the same program, 142 residues of CHCHD10 (Met1 to Pro142) were modelled using CHCHD5 as a template (PDB ID: 2LQL). Swiss-Pdb Viewer 3.7 (http://www.expasy.org/spdbv) was used to analyse the CHCHD10 mutation and visualize the structure. The modelling of CHCHD10 shows: (i) a non-structured N-terminal region; (ii) a highly hydrophobic helix (Gly43 to Ala68), which may typically be an interface of interaction with an interacting protein; and (iii) the CHCH domain near the C-terminal region characterized by a CX_9C motif (Fig. 5D). The four cysteine residues (102, 112, 122 and 132) of the CHCH domain are involved in two disulphide bonds. The p.Ser59 is located in the hydrophobic N-terminal α-helix, and as the few other polar residues of this helix, it may intervene in hydrogen bonds to stabilize CHCHD10 interaction with another protein. Thus, the p.Ser59Leu mutation could possibly alter protein–protein interactions.

To investigate whether the p.Ser59Leu mutation has an effect on the expression of CHCHD10, we analysed CHCHD10 level in muscle of patients by western blotting. We used GAPDH and the mitochondrial SMAC protein (now known as DIABLO) as controls for quantitation. Normalization showed no significant reduction of CHCHD10 expression in patient muscles compared to control (not shown).

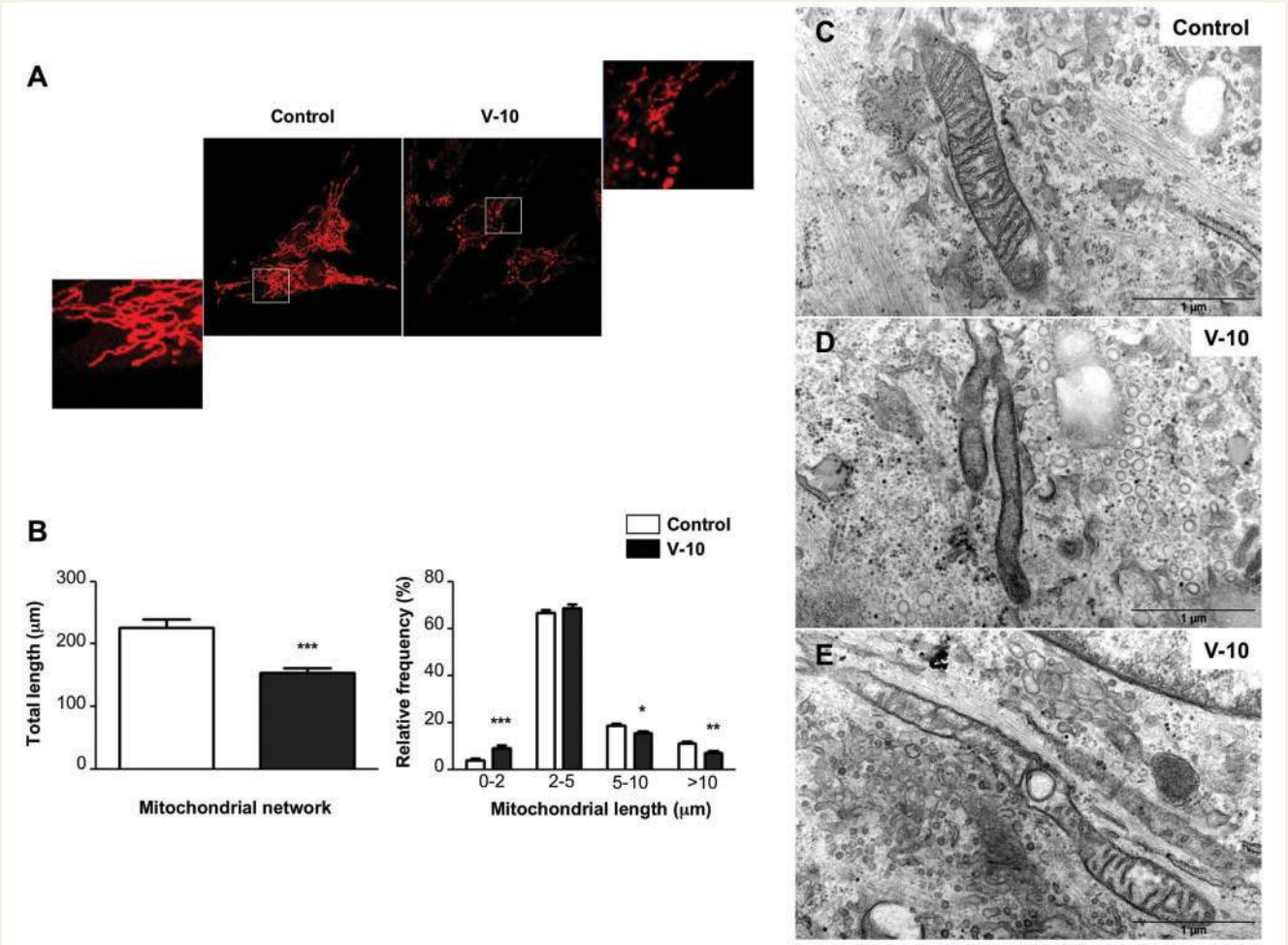

Figure 3 Mitochondrial fragmentation and ultrastructural alterations in skin fibroblasts. (**A**) Cells obtained from a control (*left*) and Patient V-10 (*right*) were analysed by confocal microscopy using MitoTracker® Red. Enlarged details of the areas are indicated. (**B**) Mitochondrial phenotypes showed in **A** were quantified for 35 randomly-selected individual cells per each studied fibroblast cell line from two independent experiments. The data obtained were used to calculate the total length of the mitochondrial network per cell (*left*) and the average mitochondrial fragment length (*right*). Differences between the two cell lines were analysed by Student's *t*-test: significant ($*0.05 > P > 0.01$), very significant ($**0.01 > P > 0.001$) or extremely significant ($***P < 0.001$). (**C–E**) Ultrastructural analysis of control (**C**) and Patient V-10 (**D** and **E**) fibroblasts. Scale bar = 1 μm (**C**) Representative image of mitochondria with typical normal aspect found in control cells. (**D**) Complete mitochondrial disorganization only found in patient cells. (**E**) Moderate disorganization mainly found in patient cells.

CHCHD10 is a mitochondrial protein located in the intermembrane space

First, we looked at the expression of CHCHD10 in human tissues by western blot. The protein is ubiquitous and highly expressed in organs with high mitochondrial content such as the heart or liver (Fig. 6A). Confocal microscopic analysis showed a co-localization, in HeLa cells, of endogenous CHCHD10 with MitoTracker®, a dye that accumulates specifically in mitochondria (Fig. 6B). To analyse sub-mitochondrial localization of CHCHD10, mitochondria isolated from HeLa cells were treated with proteinase K. Proteins inside mitochondria are protected from protease digestion. As shown in Fig. 6C, CHCHD10 was resistant to treatment with proteinase K indicating that the protein is present inside mitochondria. As expected, the TOMM20 protein (outer mitochondrial membrane) was digested by proteinase K whereas SMAC (intermembrane space) was resistant to protease digestion. Analysis of the mitochondrial preparations for PCNA and GAPDH confirmed the absence of nuclear and cytosolic contaminations, respectively. When mitochondria were subjected to alkali extraction, peripheral membrane proteins were recovered in the supernatant, whereas integral membrane proteins were found in the membrane-containing pellet fractions (Fig. 6D). As expected, the outer membrane integral protein VDAC1 was primarily recovered in the pellet after extraction whereas SMAC was recovered in the supernatant. CHCHD10 was distributed in the supernatant indicating that it was located in the soluble fraction. Last, to discriminate between intermembrane space or matrix localization, mitochondria were treated with digitonin to open the inner membrane space. In the resulting mitoplasts,

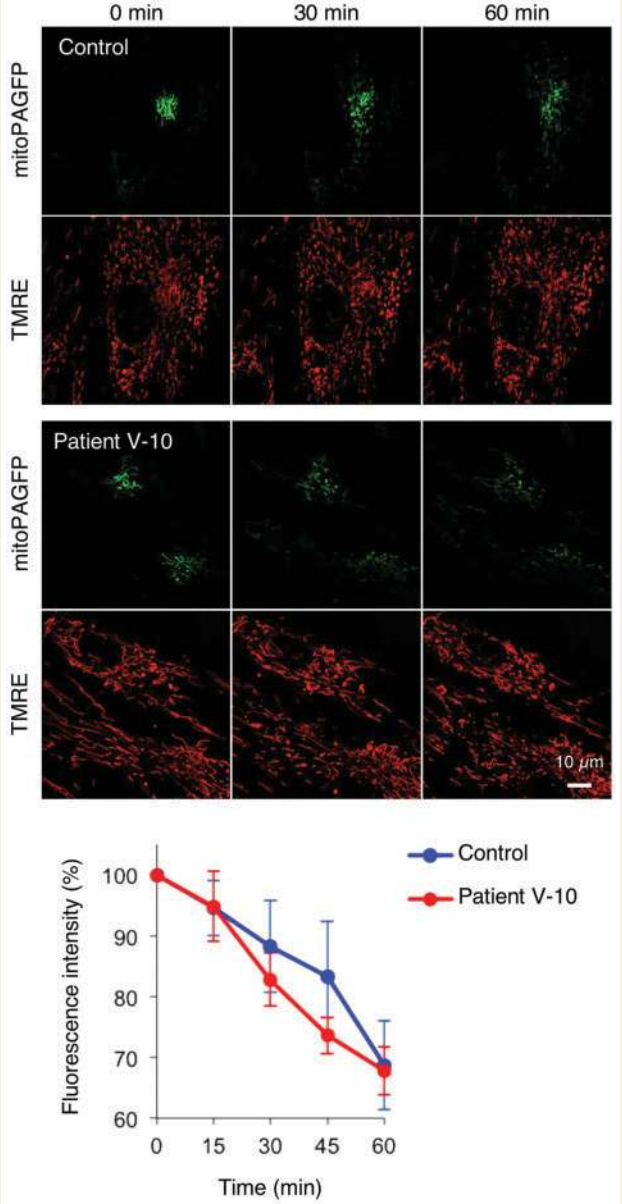

Figure 4 Fusion analysis in patient fibroblasts. Control and patient fibroblasts expressing mitochondria-targeted photoactivatable GFP (mitoPAGFP) were stained with 7 nM tetramethylrhodamine ethyl ester (TMRE). mitoPAGFP was photoactivated with a 405-nm laser in a small region of cells (30 × 30 pixels) at 0 min. Fibroblasts were observed with 15-min intervals for 60 min. Fluorescence intensity of mitoPAGFP was quantified using NIH ImageJ. Values represent the mean ± SEM ($n = 7$ for controls and $n = 9$ for patients).

CHCHD10 was degraded by proteinase K like MFN2 (outer mitochondrial membrane), SMAC (intermembrane space) and IMMT, an inner mitochondrial membrane protein mainly facing the intermembrane space, whereas HSPD1 (Hsp60), which is located in the mitochondrial matrix, was protected against protease digestion (Fig. 6E). All these results suggest that CHCHD10 is an intermembrane space protein.

CHCHD10 is enriched at cristae junctions

We performed immunogold labelling of chemically fixed cryosectioned HeLa cells (Fig. 7A). The sections were labelled with a primary antibody against CHCHD10, followed by a secondary gold conjugate. For quantitative analysis, we determined the location of each gold particle ($n = 229$) with respect to the inner boundary membrane and the closest cristae membrane and plotted its respective localization in a model (Fig. 7B). We found that the majority of mitochondrial gold particles were enriched in the vicinity of cristae junctions as reported previously for IMMT, a major component of the MINOS (mitochondrial inner membrane organizing system) complex (Jans *et al*., 2013). We performed the same experiment with a primary antibody against HSPD1 (Hsp60), a protein highly expressed in the matrix, as a control (Fig. 7C and D).

Expression of CHCHD10 mutant leads to fragmentation of the mitochondrial network and to defect in cristae maintenance

To confirm the role of the p.Ser59Leu mutation, we analysed the effects of overexpression of the pathogenic allele on mitochondrial network. HeLa cells were transiently transfected with the empty vector, the wild-type allele or the pathological allele. After transfection, HeLa cells produced equivalent amounts of wild-type and mutant CHCHD10 (Fig. 8A). Mitochondrial network morphology and CHCHD10 labelling were next assessed using MitoTracker® red and CHCHD10 antibodies, respectively. Forty-eight hours after transfection with either empty vector or the wild-type allele, MitoTracker® revealed a filamentous network. Overexpression of mutant CHCHD10^{S59L} altered mitochondrial morphology in transfected cells with a significant fragmentation of the network (Fig. 8B and C). We also looked at the mitochondrial morphology by electron microscopy. Contrary to overexpression of either empty vector or the wild-type allele, overexpression of the CHCHD10^{S59L} mutant led to major abnormalities including loss, disorganization or dilation of cristae. Matrix condensation was also observed in numerous mitochondria (Fig. 9A–D).

Involvement of the same *CHCHD10* mutation in a frontotemporal dementia-amyotrophic lateral sclerosis family

The observation of a FTD-ALS phenotype in a mitochondrial disease led us to analyse *CHCHD10* in a cohort of 21 FTD-ALS families previously tested by exome sequencing. We identified the heterozygous c.176C>T (p.Ser59Leu) mutation in a patient whose family is originally from Catalonia (Spain). This male patient developed walking difficulties at 57 years of age. Progressively, he presented a pseudobulbar syndrome with dysarthria and dysphagia. Electromyography confirmed motor neuron involvement with symmetrical denervation predominant in muscles of the face but

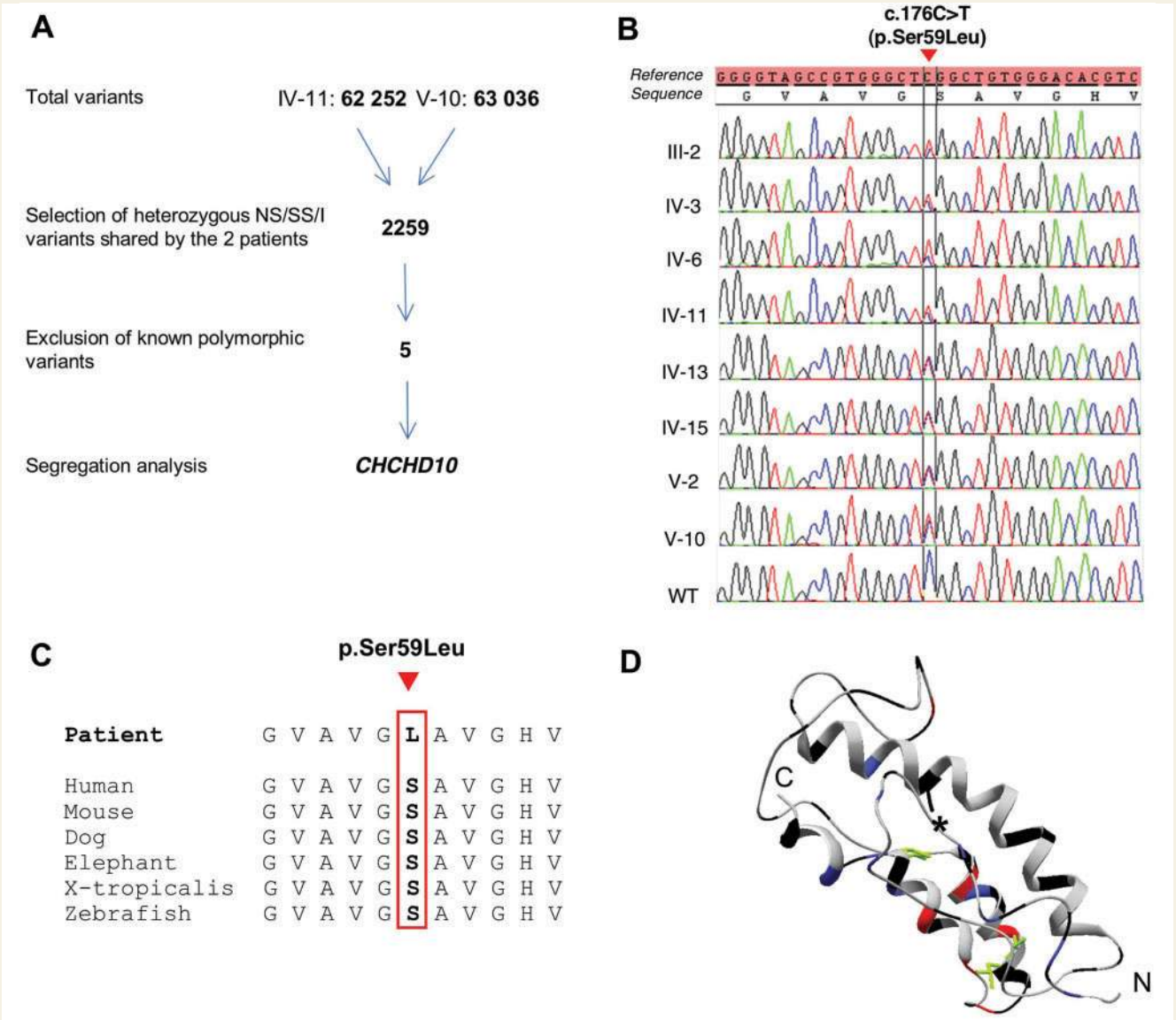

Figure 5 Identification of the p.Ser59Leu mutation in *CHCHD10*. (**A**) Schematic representation of the exome data analysis and data filtering. NS = non-synonymous variants; SS = splice site disrupting single nucleotide variants; I = exonic indels. Known variants correspond to single nucleotide polymorphisms and Indels already reported in dbSNP132, EVS (Exome Variant Server), HapMap, 1000 Genome databases and in-house control exomes. (**B**) *CHCHD10* mutation sequences in Patients III-2, IV-3, IV-6, IV-11, IV-13, IV-15, V-2, V-10 and a control (WT). (**C**) Cross-species protein conservation of CHCHD10, flanking the altered amino acid p.Ser59. (**D**) Model of CHCHD10 based on the CHCHD5 structure (PDB ID: 2LQL). Aliphatic, polar, basic and acidic residues are respectively in grey, black, blue and red. Disulphide bonds are in green. The polar residue Ser59 is indicated with an asterisk.

also in muscles of upper and lower limbs. Motor and sensory conduction velocities were normal. The patient also had cognitive impairment and behavioural changes suggesting a frontotemporal dementia. Neuropsychological testing revealed a frontal lobe dysfunction, notably impairment of conceptualization, perseverative behaviours and paraphasia with relative preservation of memory. Brain MRI showed mild bilateral frontal atrophy. Parkinsonian signs were also present with akinesia, rigidity and gait disorders and a Unified Parkinson's Disease Rating Scale at 10. In addition, the patient presented bilateral sensorineural hypoacousia and a muscular fatigability. A total loss of autonomy was observed after 8 years of evolution, before a loss of sight. The elder sister and one brother of the index case presented with ALS with predominant bulbar features and died after 4 years of evolution. Their father developed a neurological disease with progressive walking and speaking difficulties at 61 years of age leading to death 3 years later. No patient had a muscle biopsy. The presence of the mutation was confirmed by Sanger method in the index case but the absence of DNA samples from other family members did not allow us to perform segregation analysis.

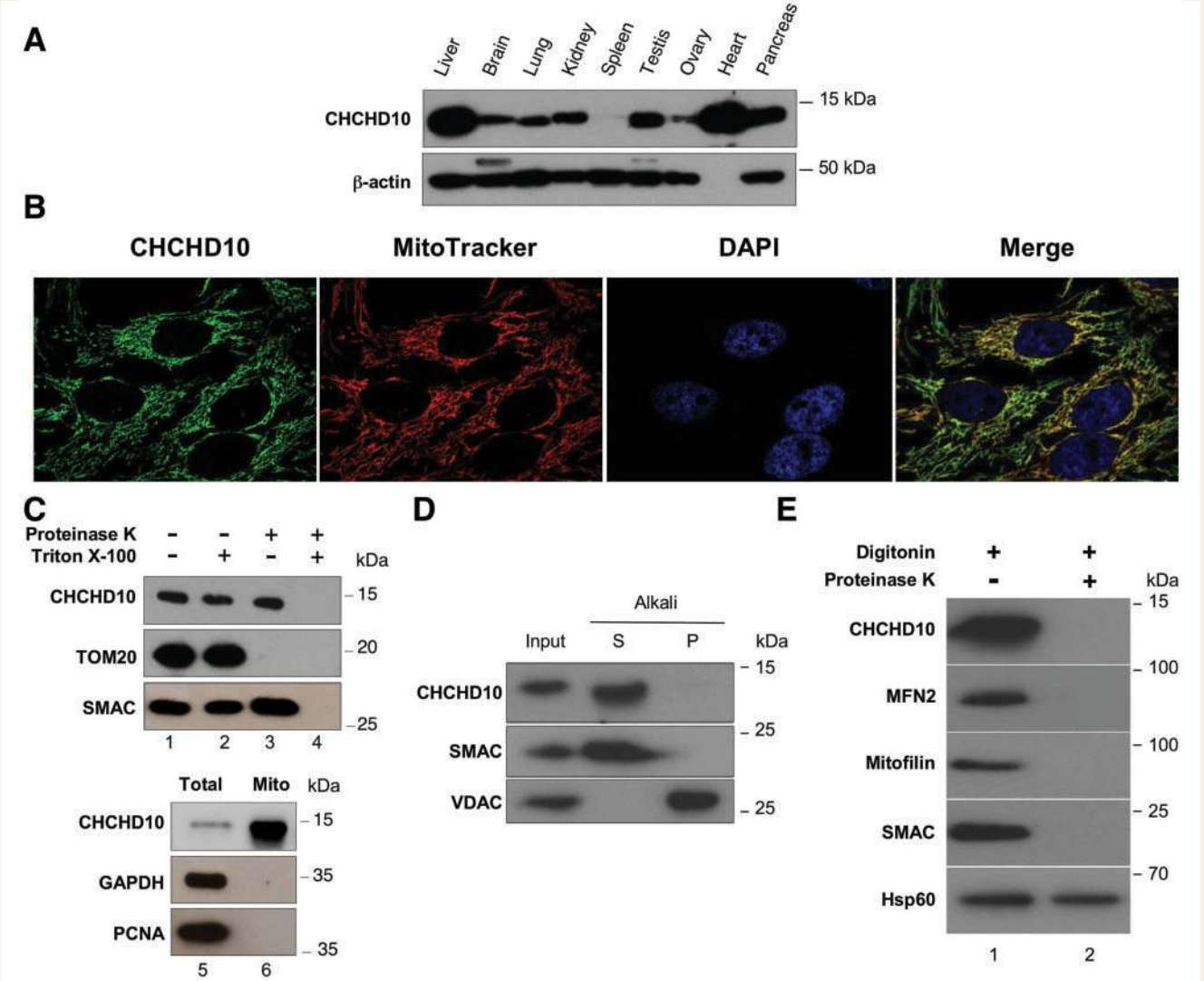

Figure 6 Mitochondrial localization of CHCHD10. (**A**) Expression of CHCHD10 protein in human tissues analysed by western blotting using human multiple tissue blot. (**B**) Co-localization of endogenous CHCHD10 protein with MitoTracker® Red indicating mitochondrial localization for CHCHD10 in HeLa cells (overlay in yellow). (**C**) Intact isolated mitochondria from HeLa cells (lanes 1–4) were incubated in presence (+) or in absence (-) of proteinase K or Triton™ X-100 before analysis by immunoblotting using antibodies against CHCHD10, TOMM20 (mitochondrial outer membrane protein) or SMAC (mitochondrial intermembrane space protein). To verify the purity of isolated mitochondria, total lysates (lane 5) and mitochondrial isolates (lane 6) were analysed by immunoblotting using antibodies against CHCHD10, GAPDH (cytosolic protein) or PCNA (nuclear protein). (**D**) Intact mitochondria were prepared and subjected to Na_2CO_3 extraction. A soluble protein fraction (S) and an integral membrane protein fraction (P) were prepared. Samples of an extract from intact mitochondria (input), and the fraction of each extraction were subjected to western blot analysis. VDAC1 and SMAC were used to identify behaviours of well-defined mitochondrial proteins that are integral membrane protein and soluble, respectively. (**E**) Isolated mitochondria from HeLa cells (lanes 1 and 2) were incubated in presence (+) or in absence (-) of digitonin or proteinase K before analysis by immunoblotting using antibodies against CHCHD10, MFN2 (outer membrane protein), mitofilin (inner membrane protein mainly facing the intermembrane space, now known as IMMT), SMAC (intermembrane space protein) or Hsp60 (mitochondrial matrix protein, HSPD1).

Discussion

In this study, we first identified a new gene involved in mitochondrial DNA instability disease. We describe a large family in which affected individuals carry a missense mutation in the *CHCHD10* gene. The clinical phenotype associated with this *CHCHD10* mutation is unusual because patients developed a late-onset disease, which begins around age 50, with highly variable clinical presentations. Affected individuals presented with either isolated or associated symptoms including ataxia, dementia and ALS-like presentation; the only element common to all patients being the presence of a mitochondrial myopathy with numerous ragged-red and COX-negative fibres associated with multiple mitochondrial DNA deletions. None of the affected individuals presented with

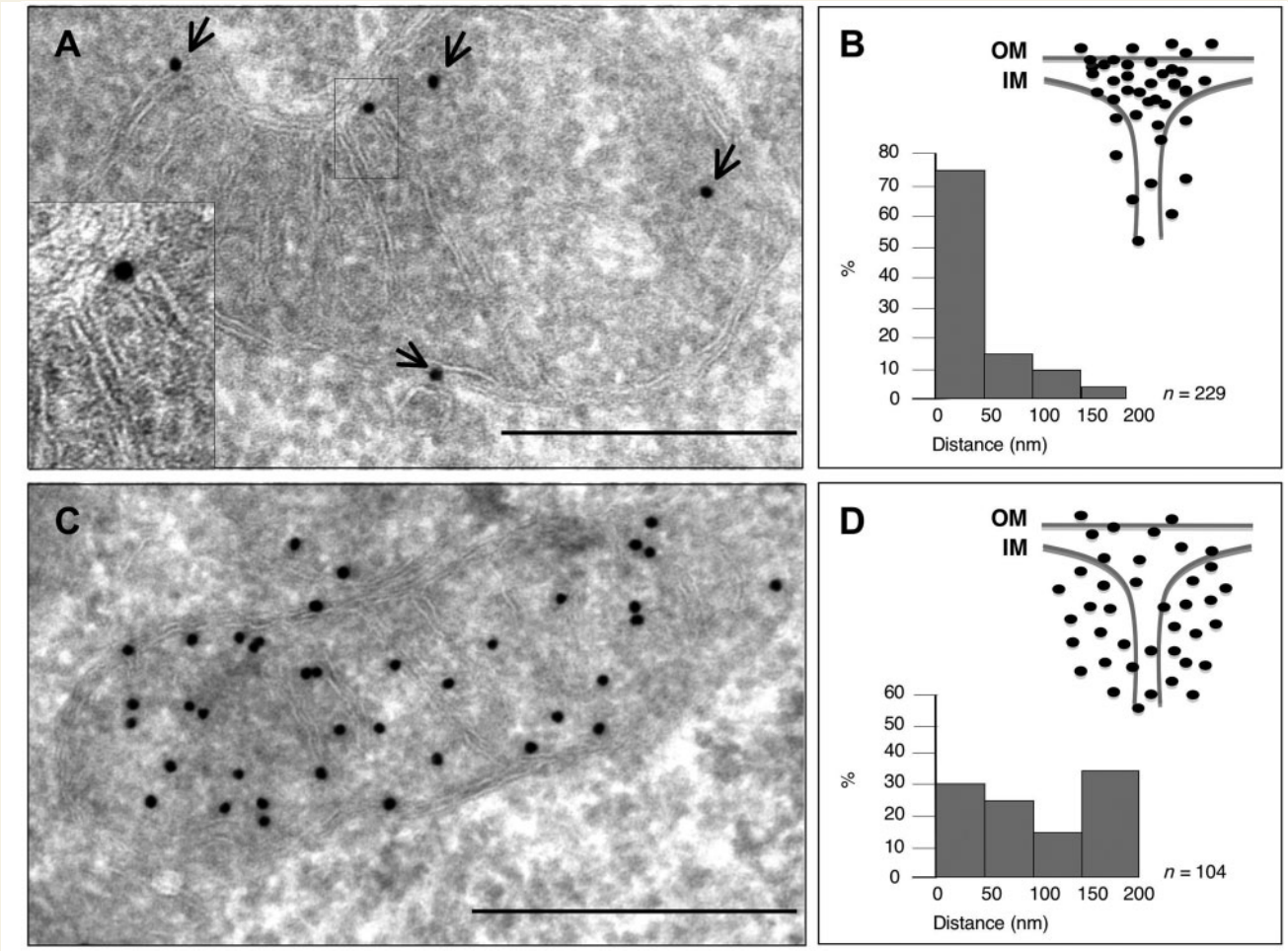

Figure 7 Submitochondrial localization of CHCHD10 using immunoelectron microscopy. (**A**) Immunogold labelling of CHCHD10 in HeLa cells. Arrows point to the position of gold particles. Enlarged details of the areas are indicated by black boxes. Scale bar = 500 nm. (**B**) Localization of the gold particles as determined by immunogold labelling of CHCHD10 plotted on a scheme representing a part of a mitochondrion. OM = outer membrane; IM = inner membrane. The histogram shows the fraction of gold particules within the indicated distance to the cristae junction. The histogram and the graphical representation are based on the same measured gold particle localizations. (**C**) Control immunogold labelling of Hsp60 in HeLa cells. Scale bar = 500 nm. (**D**) Localization of the gold particles as determined by immunogold labelling of Hsp60 plotted on a scheme representing a part of a mitochondrion. The histogram shows the fraction of gold particles within the indicated distance to the cristae junction. The histogram and the graphical representation are based on the same measured gold particle localizations.

an external ophthalmoplegia. One patient (Patient IV-15) only presented with a ptosis associated with facial palsy, probably due to motor neuron disease. In this family, the phenotype is really particular compared to those reported in mitochondrial DNA instability disorders. The course of the disease was highly variable, ranging from 1 to >15 years of evolution before death. However, it was more severe than the progressive external ophthalmoplegia phenotypes classically observed in pedigrees with autosomal dominant transmission of multiple mitochondrial DNA deletions (Copeland, 2012). Cerebellar ataxia is exceptionally observed in the absence of progressive external ophthalmoplegia in mitochondrial DNA instability disease, except in MIRAS (mitochondrial recessive ataxic syndrome) or MSCAE (mitochondrial spinocerebellar ataxia and epilepsy) phenotypes (Copeland, 2012), secondary to *POLG* mutations, or in IOSCA (infantile onset spinocerebellar ataxia) (Hakonen *et al*., 2007), secondary to *C10orf2* (twinkle) mutations. Motor neuron disease with ALS-like symptoms is even rarer with exceptional cases associated with *POLG*, *TK2* or *DGUOK* mutations (Ronchi *et al*., 2012). The cognitive impairment observed in our family resembles FTD usually observed in patients with ALS. This observation led us to analyse *CHCHD10* in FTD-ALS families with a dominant mode of transmission and to identify the same missense p.Ser59Leu mutation in one of these families. FTD-ALS is a genetically heterogeneous disorder and a hexanucleotide repeat expansion in a non-coding region of the *C9orf72* gene, the function of which is unknown, has been recently identified as a common cause of FTD-ALS (DeJesus-Hernandez *et al.*, 2011; Renton *et al.*, 2011). Patients with a *C9orf72* expansion present with FTD, ALS, or both. Parkinsonism is common and the phenotype of our second family was highly evocative of a *C9orf72* expansion. However, *C9orf72* screening and the analysis of other candidate genes for

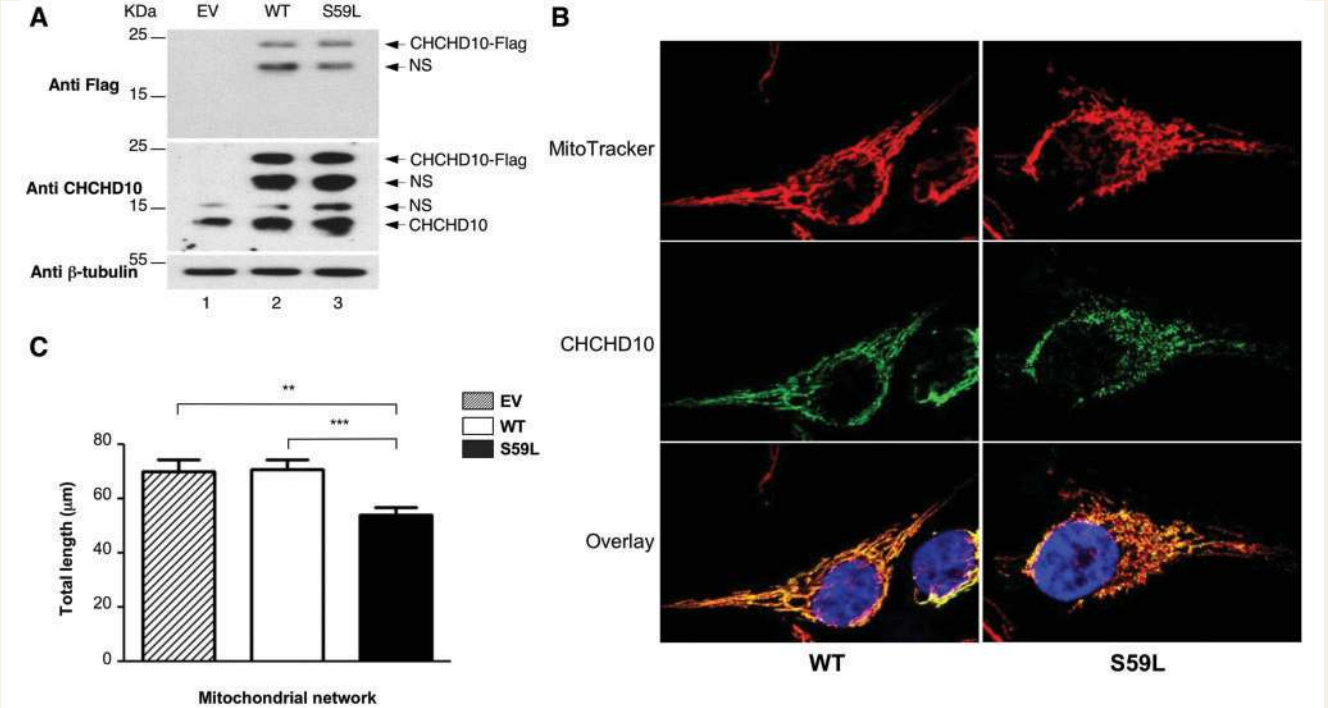

Figure 8 Effects of overexpression of wild-type and pathogenic *CHCHD10* alleles on mitochondrial network in HeLa cells. Transfections were performed with empty vector (EV) or vectors encoding either wild-type CHCHD10-Flag (WT) or mutant CHCHD10-Flag (S59L). (**A**) Western blot of HeLa cell extracts using antibodies against Flag, CHCHD10 or β-tubulin. NS = non-specific. (**B**) Analysis of DAPI (blue), MitoTracker® (red) staining and CHCHD10 (green) immunolabelling by fluorescence microscopy in HeLa cells transfected with either wild-type CHCHD10-Flag (WT) or mutant CHCHD10-Flag (S59L). (**C**) Quantification of mitochondrial phenotypes of cells transfected with empty vector (EV) or vectors encoding either wild-type CHCHD10-Flag (WT) or mutant CHCHD10-Flag (S59L). Thirty-five randomly-selected individual cells per each transfection were analysed from two independent experiments. The data obtained were used to calculate the total length of the mitochondrial network per cell. Differences between the two cell lines were analysed by Student's *t*-test: very significant (**: $0.01 > P > 0.001$) or extremely significant (***: $P < 0.001$).

ALS and FTD were negative in this family (*TARDBP*, *FUS/TLS*, *SOD1*, *VCP*, *CHMP2B*, *ANG*, *SQSTM1*, *UBQLN2*, *PFN1*). No patient had a muscle biopsy, but it is likely that sensorineural hypoacousia and muscle weakness observed in the index case were related to mitochondrial dysfunction. Our study clearly shows that *CHCHD10* is a novel gene responsible for ALS-FTD clinical spectrum, which raises the intriguing prospect of an underlying mitochondrial basis for this group of disorders.

The function of CHCHD10 is unknown. However, it belongs to a family of mitochondrial proteins characterized by conserved CX_nX motifs (Banci *et al*., 2009) and it is expected to be involved in oxidative phosphorylation (Martherus *et al.*, 2010). These proteins are incorporated into the intermembrane space and are then trapped through a redox-dependent protein machinery through the intermembrane space protein Mia 40 (CHCHD4) (Stojanovski *et al*., 2012). CHCHD3 is a member of this family predominantly localized to the inner membrane, facing toward the intermembrane space (Darshi *et al*., 2012). It is part of the large protein complex called MINOS and plays a role in maintaining mitochondrial function and cristae integrity (Darshi *et al*., 2011; van der Laan *et al*., 2012). OPA1 has been shown to be involved in regulating cristae remodelling independently of its role in mitochondrial fusion (Frezza *et al*., 2006). CHCHD3 interacts both with OPA1 and mitofilin suggesting that it is a scaffolding protein that stabilizes complexes involved in maintening cristae architecture (Darshi *et al*., 2011). Another member of this family, CHCM1/CHCHD6, is critical for maintaining the cristae morphology, ATP production and oxygen consumption. It has the same localization than CHCHD3 and strongly interacts with IMMT (An *et al*., 2012). Here, we show that CHCHD10 is a mitochondrial protein, located in the intermembrane space. Unlike CHCHD3 and/CHCHD6 (also known as CHCM1), which are inner membrane-associated proteins, CHCHD10 is a soluble protein. By electron microscopy, we also show that it is enriched at cristae junctions, like IMMT, suggesting that it could be another factor in maintaining cristae morphology. The cristae alterations found both in patient fibroblasts and HeLa cells overexpressing $CHCHD10^{S59L}$ mutant are also in favour of this hypothesis. There is strong evidence that the mitochondrial F_1F_0-ATP synthase, apart from its enzymatic activity, plays a major role in determining the structure of cristae (Zick *et al*., 2009). The regular arrangement of this highly abundant protein complex might serve as a kind of backbone stabilizing tubular cristae structures. On the contrary, we could ask whether the abnormal pattern observed for F_1F_0-ATP synthase by blue native-PAGE analysis in the muscle of patients is not secondary to an abnormal organization of cristae

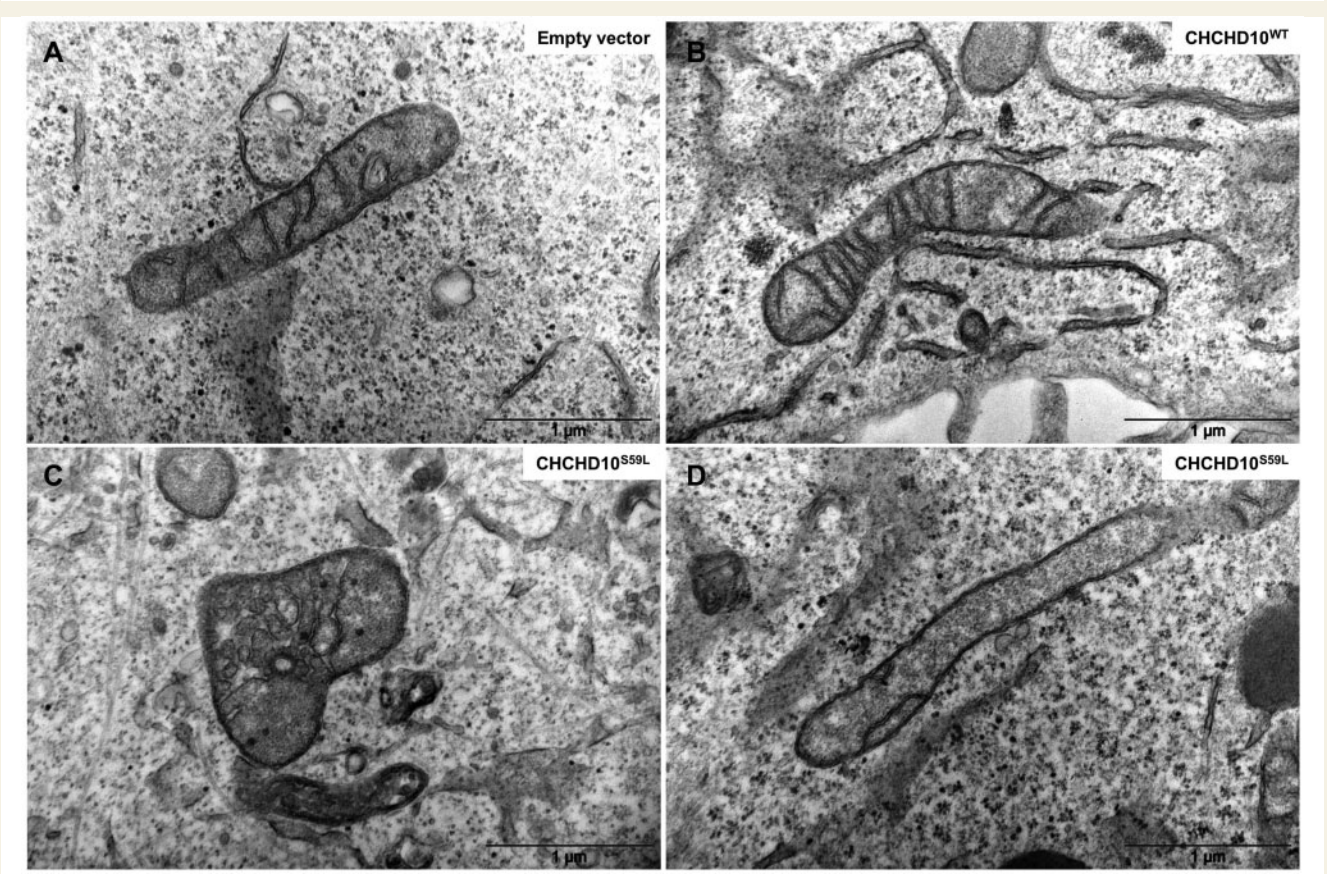

Figure 9 Effects of overexpression of wild-type and pathogenic CHCHD10 alleles on cristae morphology in HeLa cells. (**A**) Representative image of mitochondria after transfection with the empty vector. (**B**) Representative image of mitochondria in cells overexpressing the wild-type CHCHD10 allele. (**C** and **D**) Representative images of mitochondria in cells overexpressing the mutant CHCHD10 allele (S59L).

linked to the p.Ser59Leu mutation. Furthermore, this mutation leads to a respiratory chain deficiency both in muscle and fibroblasts of patients suggesting that CHCHD10 is critical for maintaining ATP production and oxygen consumption. It has been shown that cristae shape regulates respiratory chain supercomplexes' stability and assembly with an impact on mitochondrial respiratory efficiency, thus suggesting that shape of biological membranes can influence membrane protein complexes (Cogliati *et al*., 2013). Further experiments will be necessary to determine whether these effects of CHCHD10 mutant are linked to destabilization of cristae morphology.

Downregulation of both *CHCHD3* and *CHCHD6* in HeLa cells resulted in fragmentation and clustering of the mitochondrial network (Darshi *et al*., 2011; An *et al*., 2012). This could indicate either increased fission or decreased fusion in knock-out cells. Studies with the dominant negative mutant of *Drp1*, $DRP1^{K38A}$, which blocks fission, suggested that the mitochondria in CHCHD3 knock-out cells have impaired fusion activity (Darshi *et al*., 2011). Fibroblasts of patients carrying the *CHCHD10* mutated allele presented a fragmentation of the mitochondrial network and less connected mitochondria. However, a direct assay with a photoactivatable mitochondrial form of GFP did not find a mitochondrial fusion defect in patient fibroblasts. The accumulation of mitochondrial DNA deletions in skeletal muscle can be secondary to an increase in mitochondrial DNA damage, a defect in mitochondrial DNA repair and/or a failure to clear mitochondria with damaged DNA (Chen and Chan, 2010). Recently, we have shown that fibroblasts bearing a *MFN2* mutation, responsible for optic atrophy 'plus' phenotype with mitochondrial DNA multiple deletions, have a lower capacity to repair stress-induced mitochondrial DNA lesions compared to control cells (Rouzier *et al*., 2012). It is likely that the defect in mitochondrial DNA repair that we observed is due to defective fusion, which leads to a variability in repair protein content across the mitochondrial population, thus contributing to mitochondrial DNA instability. Mitochondrial DNA instability found in patients carrying the p.Ser59Leu *CHCHD10* mutation cannot be explained by a fusion deficiency. However, mammalian cells contain thousands of copies of mitochondrial DNA assembled into hundreds of nucleoids that are closely associated with the inner membrane and often appear to be wrapped around cristae or crista-like inner membrane invaginations (Brown *et al*., 2011). One cannot exclude that cristae alterations secondary to $CHCHD10^{S59L}$ expression lead to nucleoid structure disorganization and contribute to defect of mitochondrial DNA maintenance.

In conclusion, our study has provided strong supporting evidence that the CHCHD10 protein plays a role in the maintenance of mitochondrial cristae morphology and mitochondrial DNA stability. Additional work will be needed to clarify the pathogenic

mechanisms linking *CHCHD10* mutations with these downstream deleterious consequences and ultimately, the observed neurodegenerative phenotype. Moreover, this work opens a novel field to explore the pathogenesis of FTD-ALS clinical spectrum by showing that mitochondrial disease may be at the origin of some of these phenotypes. The analysis of *CHCHD10* also needs to be performed in patients presenting with ALS or FTD in both sporadic and familial cases.

Acknowledgements

We acknowledge Pasteur-IRCAN Cellular and Molecular Imaging platform (PICMI). We also acknowledge Pr François Tison (CHU Bordeaux), Cyril Goizet (CHU Bordeaux) and Pr Olivier Rascol (CHU Toulouse).

Funding

This work was made possible by grants to V.P-F from the Association Française contre les Myopathies (AFM) and the Fondation pour la Recherche Médicale (FRM), to H.S from National Institutes of Health (GM089853) and to A.B by the program 'Investissements d'avenir' ANR-10-IAIHU-06, 'The Programme Hospitalier de Recherche Clinique' (to I.L.B.) and the 7th framework program of the European Union (FP7, E12009DD, Neuromics). P.YWM is supported by a Clinician Scientist Fellowship Award (G1002570) from the Medical Research Council (UK).

References

Amati-Bonneau P, Valentino M, Reynier P, Gallardo M, Bornstein B, Boissière A, et al. *OPA1* mutations induce mitochondrial DNA instability and optic atrophy 'plus' phenotype. Brain 2008; 131: 338–51.

An J, Shi J, He Q, Lui K, Liu Y, Huang Y, et al. CHM1/CHCHD6, a novel mitochondrial protein linked to regulation of mitofilin and mitochondrial cristae morphology. J Biol Chem 2012; 287: 7411–26.

Banci L, Bertini I, Ciofi-Baffoni S, Tokatlidis K. The coiled coil-helix coil-helix proteins may be redox proteins. FEBS Lett 2009; 583: 1699–702.

Banci L, Bertini I, Coffi-Baffoni S, Jaiswal D, Peruzzini R, Winkelman J. Structural characterization of CHCHD5 and CHCHD7: two atypical twin CX9C proteins. J Struct Biol 2012; 180: 190–200.

Bannwarth S, Figueroa A, Fragaki K, Destroismaisons L, Lacas-Gervais S, Lespinasse F, et al. The human *MSH5* (MutS Homolog 5) gene localizes to mitochondria and protects the mitochondrial genome from oxidative damage. Mitochondrion 2012; 12: 654–65.

Bradford M. A rapid and sensitive method for the quantitation of micrograms quantities of protein utilizing the principle of protein-dye binding. Anal Biochem 1976; 251: 69–72.

Brown TA, Tkachuk AN, Shtengel G, Kopek BG, Bogenhagen BF, Hess HF, et al. Superresolution fluorescence imaging of mitochondrial nucleoids reveals their spatial range, limits and membrane interaction. Mol Cell Biol 2011; 31: 4494–5010.

Cavallo G. Genome-wide analysis of eukaryotic twin CX9C proteins. Mol Biosyst 2010; 6: 2459–70.

Chen H, Chan D. Physiological functions of mitochondrial fusion. Ann N Y Acad Sci 2010; 1201: 21–5.

Cogliati S, Frezza C, Soriano M, Varanita T, Quintana-Cabrera R, Corrado M, et al. Mitochondrial cristae shape determines respiratory chain supercomplexes and respiratory efficiency. Cell 2013; 155: 160–71.

Copeland W. Defects in mitochondrial DNA replication and human disease. Crit Rev Biochem Mol Biol 2012; 47: 64–74.

Darshi M, Mendiola V, Mackey M, Murphy A, Koller A, Perkins G, et al. ChChd3, an inner mitochondrial membrane protein, is essential for maintening crista integrity and mitochondrial function. J Biol Chem 2011; 286: 2918–32.

Darshi M, Trinh K, Murphy A, Taylor S. Targeting and import mechanism of coiled-coil helix coiled-coil helix domain-containing protein 3 (ChChd3) into the mitochondrial intermembrane space. J Biol Chem 2012; 287: 39480–91.

DeJesus-Hernandez M, Mackenzie IR, Boeve BF, Boxer AL, Baker M, Rutherford NJ, et al. Expanded GGGGCC hexanucleotide repeat in noncoding region of C9ORF72 causes chromosome 9p-linked FTD and ALS. Neuron 2011; 72: 245–56.

Delettre C, Laeners G, Griffoin J, Gigarel N, Lorenzo C, Belenguer P, et al. Nuclear gene *OPA1*, encoding a mitochondrial dynamin-related protein, is mutated in dominant optic atrophy. Nat Genet 2000; 26: 207–10.

Frezza C, Cipolat S, Martins de Brito O, Micaroni M, Beznoussenko G, Rudka T, et al. OPA1 controls apoptotic cristae remodeling independently from mitochondrial fusion. Cell 2006; 126: 177–89.

Hakonen A, Isohanni P, Paetau A, Herva R, Suomalainen A, Lonngvist T. Recessive Twinkle mutations in early onset encephalopathy with mtDNA depletion. Brain 2007; 130: 3032–40.

Hudson G, Amati-Bonneau P, Blakely E, Stewart J, He L, Schaefer A, et al. Mutation of *OPA1* causes dominant optic atrophy with external ophtalmoplegia, ataxia, deafness, and multiple mitochondrial DNA deletions: a novel disorder of mtDNA maintenance. Brain 2008; 131: 329–37.

Jans D, Wurm C, Riedel D, Wenzel D, Stagge F, Deckers M, et al. STED super-resolution microscopy reveals an array of MINOS clusters along human mitochondria. PNAS 2013; 110: 8936–41.

Karbowski M, Arnoult D, Chen H, Chan DC, Smith CL, Youle RJ. Quantitation of mitochondrial dynamics by photolabeling of individual organelles shows that mitochondrial fusion is blocked during the Bax activation phase of apoptosis. J Cell Biol 2004; 164: 493–9.

Kelley L, Sternberg M. Protein structure prediction on the web: a case study using the Phyre server. Nat Protoc 2009; 4: 363–71.

Kim JS, Xu X, Li H, Solomon D, Lane WS, Jin T, et al. Mechanistic analysis of a DNA damage-induced, PTEN-dependent size checkpoint in human cells. Mol Cell Biol 2011; 31: 2756–71.

Koshiba T, Detmer S, Kaiser J, Chen H, McCaffery M, Chan D. Structural basis of mitochondrial tethering by mitofusin complexes. Science 2004; 305: 858–62.

Longen S, Bien M, Bihlmaier K, Kloeppel C, Kauff F, Hammermeister M, et al. Systematic analysis of the twin cx(9)c protein family. J Mol Biol 2009; 393: 356–68.

Martherus RS, Sluiter W, Timmer ED, VanHerle SJ, Smeets HJ, Ayoubi TA. Functional annotation of heart enriched mitochondrial genes GBAS and CHCHD10 through guilt by association. Biochem Biophys Res Com 2010; 402: 203–8.

Meeusen S, McCaffery M, Nunnari J. Mitochondrial fusion intermediates revealed *in vitro*. Science 2004; 305: 1747–52.

Moraes C, DiMauro S, Zeviani M, Lombes A, Shanske S, Miranda A, et al. Mitochondrial DNA deletions in progressive external ophtalmoplegia and Kearns-Sayre syndrome. N Engl J Med 1989; 18: 1293–9.

Naimi M, Bannwarth S, Procaccio V, Pouget J, Desnuelle C, Pellissier J, et al. Molecular analysis of *ANT1, TWINKLE* and *POLG* in patients with multiple deletions or depletion of mitochondrial DNA by dHPLC-based assay. Eur J Hum Genet 2006; 14: 917–22.

Paul R, Santucci S, Saunières S, Desnuelle C, Paquis-Flucklinger V. Rapid mapping of mitochondrial DNA deletions by large-fragment PCR. Trends Genet 1996; 12: 131–2.

Renton AE, Majounie E, Waite A, Simon-Sanchez J, Rollinson S, Gibbs JR, et al. A hexanucleotide repeat expansion in C9ORF72 is the cause of chromosome 9p21-linked ALS-FTD. Neuron 2011; 72: 257–68.

Ronchi D, Garone C, Bordoni A, Rios PG, Calvo SE, Ripolone M, et al. Next-generation sequencing reveals *DGUOK* mutations in adult patients with mtDNA deletions. Brain 2012; 135: 3404–15.

Rouzier C, Bannwarth S, Chaussenot A, Chevrollier A, Verschueren A, Bonello-Palot N, et al. The *MFN2* gene is responsible for mitochondrial DNA instability and optic atrophy 'plus' phenotype. Brain 2012; 135: 23–34.

Rouzier C, Le Guédard-Méreuze S, Fragaki K, Serre V, Miro J, Tuffery-Giraud S, et al. The severity of phenotype linked to *SUCLG1* mutations could be correlated with residual amount of SUCLG1 protein. J Med Genet 2010; 47: 670–6.

Rustin P, Chretien D, Bourgeron T, Gerard B, Rotig A, Saudubray J. Biochemical and molecular investigations in respiratory chain deficiencies. Clin Chem Acta 1994; 228: 31–51.

Schägger H, Pfeiffer K. The ratio of oxidative phosphorylation complexes I-IV in bovine heart mitochondria and the composition of respiratory chain supercomplexes. J Biol Chem 2001; 276: 37861–7.

Shapira A. Mitochondrial diseases. Lancet 2012; 379: 1825–34.

Song Z, Ghochani M, McCaffery M, Frey T, Chan D. Mitofusins and OPA1 mediate sequential steps in mitochondrial membrane fusion. Mol Biol Cell 2009; 20: 3525–32.

Stojanovski D, Bragozewski P, Chacinska A. The MIA pathway: a tight bond between protein transport and oxidative folding in mitochondria. Biochim Biophys Acta 2012; 1823: 1142–50.

Suomalainen A, Isohanni P. Mitochondrial DNA depletion syndromes-many genes, common mechanisms. Neuromuscul Disord 2010; 20: 429–37.

Tokuyasu T. A. A technique for ultracryotomy of cell suspensions and tissues. J Cell Biol 1973; 57: 551–65.

van der Laan M, Bohnert M, Wiedemann N, Pfanner N. Role of MINOS in mitochondrial membrane architecture and biogenesis. Trends Cell Biol 2012; 22: 185–92.

Wakabayashi J, Zhang Z, Wakabayashi N, Tamura Y, Fukaya M, Kensler TW, et al. The dynamin-related GTPase Drp1 is required for embryonic and brain development in mice. J Cell Biol 2009; 186: 805–16.

Ylikallio E, Suomalainen A. Mechanisms of mitochondrial disease. Ann Med 2012; 44: 41–59.

Zanna C, Ghelli A, Porcelli A, Karbowski M, Youle R, Schimpf S, et al. *OPA1* mutations associated with dominant optic atrophy impair oxidative phosphorylation and mitochondrial fusion. Brain 2008; 131: 352–67.

Zick M, Rabl R, Reichert A. Cristae formation-linking ultrastructure and function of mitochondria. Biochim Biophys Acta 2009; 1793: 5–19.

Zuchner S, Mersiyanova I, Muglia M, Bissar-Tadmouri N, Rochelle J, Dadali E, et al. Mutations in the mitochondrial GTPase mitofusin 2 cause Charcot-Marie-Tooth neuropathy type 2A. Nat Genet 2004; 36: 459–1.